

Detection of H₂ Emission from Mira B with the HST

Brian E. Wood¹, Margarita Karovska², Warren Hack³

Abstract.

We present results from our HST/STIS observations of Mira's companion (Mira B) carried out in 1999 August. Mira B is a compact object surrounded by an accretion disk at a distance of at least 70 AU from Mira. The high resolution ultraviolet spectra of Mira B obtained using STIS show that the spectral signatures of the accretion disk have changed dramatically when compared to HST observations obtained only four years earlier. The STIS UV spectrum detects numerous, narrow H₂ lines fluoresced by H I Ly α , which have never been seen previously in spectra of the Mira AB system. Furthermore, the continuum fluxes in the Mira B spectra are much lower than observed before, at least an order of magnitude when compared to the 1995 HST/FOC objective prism spectra, and lower than ever observed by IUE. These significant changes in the spectral distribution of Mira B might be due to disk instabilities or inhomogeneity in Mira A's massive wind, or a combination of the two.

1. Introduction

Mira (o Cet, HD 14386) is one of the most extensively observed variable stars, representing the prototype of the "Mira variable" class of pulsating AGB stars. Mira has a hot companion star, Mira B (VZ Cet), which is generally assumed to be a white dwarf. The emission from Mira B is probably powered by a surrounding accretion disk fed by Mira's massive wind. The primary evidence for the accretion disk is very broad UV emission lines observed by the *International Ultraviolet Explorer* (IUE) (e.g., C IV λ 1550, Si III] λ 1892, C III] λ 1909), which are believed to be from this rapidly rotating disk (Reimers & Cassatella 1985). Mira B was observed on 1999 August 2 using the Space Telescope Imaging Spectrograph (STIS) instrument on board the *Hubble Space Telescope* (HST). The observations consisted of an exposure of the 2303–3111 Å wavelength region with the E230M grating, and an exposure of the 1140–1735 Å wavelength region with the E140M grating.

¹JILA, University of Colorado

²Smithsonian Astrophysical Observatory

³Space Telescope Science Institute

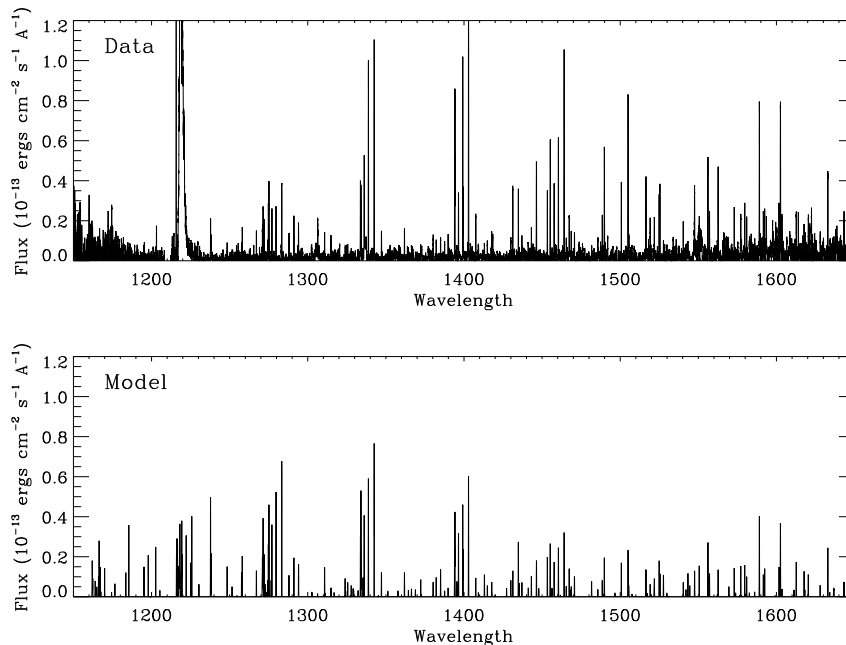


Figure 1. The top panel is a smoothed representation of the full E140M spectrum of Mira B, showing numerous narrow H_2 lines produced by $Ly\alpha$ fluorescence. The bottom panel is a fit to this spectrum assuming that the line ratios within the 13 identified fluorescence sequences are consistent with the H_2 transition probabilities. The fit is very poor, with the discrepancy possibly being due to systematically higher opacities for the low wavelength lines (see text).

2. The H_2 Lines

The top panel of Figure 1 shows the full E140M spectrum taken by HST/STIS. The spectrum is dominated by a very large number of narrow lines, which were not seen in previous IUE observations of Mira B. These are all H_2 lines fluoresced by the H I $Ly\alpha$ line (Wood, Karovska, & Hack 2001). A full list of the detected H_2 lines is provided at the end of this paper in Table 1 (Wood et al., in preparation), where the lines are grouped into 13 fluorescence sequences, representing 13 separate H_2 transitions within the $Ly\alpha$ line that are being pumped by the $Ly\alpha$ flux. Lines of H_2 fluoresced by $Ly\alpha$ have previously been detected in many other types of astrophysical objects, including the Sun (Jordan et al. 1977, 1978), red giant stars (McMurry et al. 1999), T Tauri stars (Brown et al. 1981; Valenti et al. 2000), and Herbig-Haro objects (Curiel et al. 1995).

Figure 1 compares the observed spectrum with a model spectrum that assumes that the line fluxes in the 13 fluorescence sequences are consistent with the H_2 transition probabilities of Abgrall et al. (1993). Thus, the model spectrum is a fit to the data with the primary free parameters being 13 normalization factors for the 13 sequences of lines, where the line ratios within each sequence

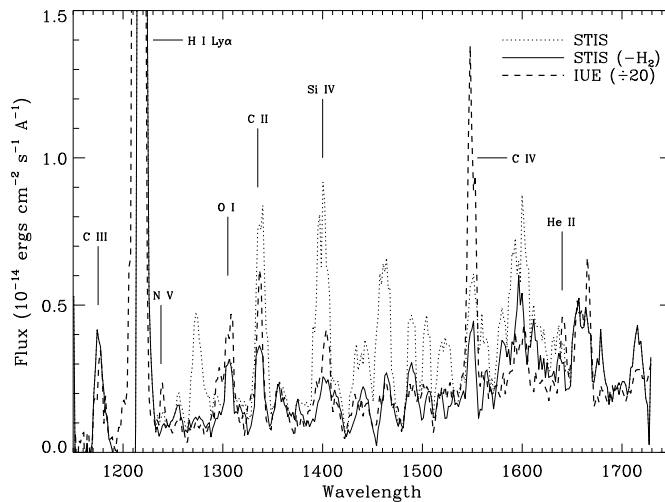


Figure 2. An IUE SWP-LO spectrum of Mira B (dashed line), displayed with line identifications, is compared with our HST/STIS spectrum (dotted line), which has been rebinned and deresolved to match the resolution of the IUE spectrum. We also show a version of the STIS spectrum deresolved after the removal of all the narrow H₂ lines (solid line). Note that the IUE fluxes had to be reduced by a factor of 20 to match the HST/STIS continuum fluxes. From Wood et al. (2001).

are assumed to be the theoretical ones. The resulting fit is not very good. The discrepancy with the data is wavelength dependent, with the shorter wavelength lines having observed fluxes that are lower relative to the longer wavelength lines than the transition probabilities predict (see Fig. 1).

We believe that this is due to an opacity effect. The lower wavelength lines are transitions to lower vibrational levels than the higher wavelength lines. The lower vibrational levels will have higher populations if the levels are thermally populated, so the lower wavelength lines should have higher opacities, thereby explaining why they have systematically lower fluxes than the model predicts.

3. Comparison with Previous Observations

The HST/STIS spectrum in Figure 1 looks radically different from what was expected based on previous IUE observations (Wood et al. 2001), all of which instead show a spectrum dominated by a few lines commonly observed in far-UV (FUV) spectra of stars and other astrophysical objects: C IV λ 1550, C II λ 1336, etc. Figure 2 shows an example of one of the low resolution IUE spectra (SWP7029) of this spectral region, with line identifications (Reimers & Cassatella 1985). We rebinned and smoothed our STIS/E140M spectrum to match the resolution of the IUE spectrum, and the result is also shown in Figure 2. To make it clear which features in the deresolved STIS spectrum are H₂ fea-

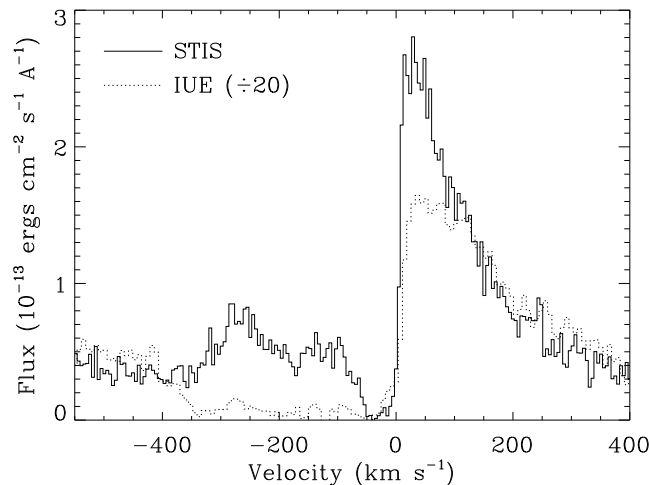


Figure 3. Comparison of the Mg II k line profile observed by HST/STIS (solid line) and one observed by IUE (dotted line). The IUE fluxes are reduced by a factor of 20 to roughly match the STIS fluxes. Note the larger wind opacity between 0 and -400 km s^{-1} in the IUE spectrum. From Wood et al. (2001).

tures, another version of the STIS/E140M spectrum is shown in Figure 2 that is rebinned and smoothed only after removing all the narrow H_2 lines.

Figure 2 emphasizes the different character of the FUV spectrum observed by STIS compared with the IUE spectra. This is due primarily to the H_2 lines, but another difference is that the continuum fluxes of the STIS spectrum are well below those detected by previous observations. The fluxes of the IUE spectrum in Figure 2 were divided by 20 to match the continuum observed by STIS. The IUE data set clearly shows some variability, but only variations of about a factor of 2 or so (Reimers & Cassatella 1985). *The STIS continuum fluxes are an order of magnitude lower than any of the IUE spectra.* This result extends to the near-UV (NUV) spectral region as well. The STIS NUV fluxes are at least an order of magnitude lower than the all the IUE observations, and they are also a factor of 10 lower than NUV fluxes observed in 1995 in an HST Faint Object Camera (FOC) PRISM spectrum (Karovska et al. 1997).

Finally, in Figure 3 the Mg II k line profile observed by STIS is compared with a typical LW-HI observation from IUE (Wood et al. 2001). The IUE fluxes are once again divided by 20 to roughly match the STIS fluxes. In the IUE profile, an opaque absorption feature is observed between 0 and -400 km s^{-1} that is indicative of a high speed wind from Mira B. The extent of the absorption varies within the IUE data set, but the wind absorption is always opaque out to at least -200 km s^{-1} . The STIS profile is different in that the absorption is only opaque to -50 km s^{-1} , and the absorption between 0 and -50 km s^{-1} could be entirely interstellar. There *is* clearly wind absorption on the blue side of the STIS Mg II profile, but the wind opacity is much less than in any of the

IUE spectra. This suggests that Mira B's wind was much weaker at the time of the STIS observations than when IUE observed the star.

4. Discussion

Perhaps the most important question regarding the H₂ lines in the UV spectrum of Mira B is, where are they coming from? The fluoresced H₂ may be located in the cool outer regions of the accretion disk surrounding Mira B, or perhaps the H₂ is in Mira A's slow, cool wind, which is fluoresced as it approaches the hot companion star and interacts with its faster wind.

The fluxes in the HST/STIS observations of Mira B's UV spectrum are dramatically lower than ever observed before by IUE or HST. Something must have happened to reduce the accretion rate onto the companion, thereby significantly lowering the accretion luminosity. The lower accretion rate leads to a lower mass loss rate from Mira B, based on the Mg II profiles (see Fig. 3). It is uncertain what caused the accretion rate to change. Instabilities in the accretion disk could be responsible. More luminous accretion systems such as dwarf novae and cataclysmic variables show dramatic variability. Inhomogeneities in the wind of Mira A might also be responsible, as it is this wind that feeds the accretion disk and there is evidence for substantial inhomogeneity in Mira A's massive wind (Lopez et al. 1997).

A final fundamental question is why the lower accretion rate is also accompanied by more prominent emission from H₂ lines. The lower accretion luminosity and weaker wind might allow more H₂ molecules to exist close to Mira B, resulting in more fluorescence from Mira B's broad Ly α emission. Future more detailed analysis and modeling of the very rich H₂ fluorescence spectrum should shed some light on this issue.

References

- Abgrall, H. A., Roueff, E., Launay, F., Roncin, J. -Y., & Subtil, J. -L. 1993, *A&AS*, 101, 273
- Brown, A., Jordan, C., Millar, T. J., Gondhalekar, P., & Wilson, R. 1981, *Nature*, 290, 34
- Curiel, S., Raymond, J. C., Wolfire, M., Hartigan, P., Morse, J., Schwartz, R. D., & Nisenson, P. 1995, *ApJ*, 453, 322
- Jordan, C., Brueckner, G. E., Bartoe, J.-D. F., Sandlin, G. D., & VanHoosier, M. E. 1977, *Nature*, 270, 326
- Jordan, C., Brueckner, G. E., Bartoe, J.-D. F., Sandlin, G. D., & VanHoosier, M. E. 1978, *ApJ*, 226, 687
- Karovska, M., Hack, W., Raymond, R., & Guinan, E. 1997, *ApJ*, 482, L175
- Lopez, B., et al. 1997, *ApJ*, 488, 807
- McMurry, A. D., Jordan, C., & Carpenter, K. G. 1999, *MNRAS*, 302, 48
- Reimers, D., & Cassatella, A. 1985, *ApJ*, 297, 275
- Valenti, J. A., Johns-Krull, C. M., & Linsky, J. L. 2000, *ApJS*, 129, 399
- Wood, B. E., Karovska, M., & Hack, W. 2001, *ApJ*, 556, L51

Table 1
Detected H₂ Lines

ID	λ_{rest} (Å)	Flux (10 ⁻¹⁵)	ID	λ_{rest} (Å)	Flux (10 ⁻¹⁵)	ID	λ_{rest} (Å)	Flux (10 ⁻¹⁵)
Fluoresced by 1-2 R(6) λ 1215.7263			Fluoresced by 4-0 P(19) λ 1217.4100			Fluoresced by 0-2 R(2) λ 1219.0887		
1-2 P(8)	1237.8623	1.70 ± 0.39	4-1 P(19)	1266.8791	2.23 ± 0.39	0-3 P(4)	1287.7306	1.93 ± 0.34
1-3 P(8)	1293.8674	2.85 ± 0.42	4-4 P(19)	1414.6960	1.52 ± 0.33	0-4 P(4)	1346.9081	2.27 ± 0.35
1-6 P(8)	1467.0791	4.15 ± 0.56	4-2 R(17)	1274.0330	1.46 ± 0.34	0-5 P(4)	1407.2856	3.93 ± 0.50
1-7 P(8)	1524.6484	5.99 ± 0.74	4-4 R(17)	1372.0611	1.20 ± 0.35	0-6 P(4)	1468.3873	2.37 ± 0.46
1-8 P(8)	1580.6660	4.24 ± 0.88	4-6 R(17)	1465.1862	1.98 ± 0.41	0-3 R(2)	1276.3223	0.71 ± 0.26
1-3 R(6)	1271.0135	2.42 ± 0.47	Fluoresced by 0-2 R(1) λ 1217.6426			0-4 R(2)	1335.1300	0.88 ± 0.27
1-4 R(6)	1327.5595	0.58 ± 0.35	0-3 P(3)	1283.1111	5.89 ± 0.62	0-5 R(2)	1395.1965	1.20 ± 0.29
1-6 R(6)	1442.8602	2.87 ± 0.45	0-4 P(3)	1342.2559	18.88 ± 1.00	Fluoresced by 2-2 R(9) λ 1219.1005		
1-7 R(6)	1500.4424	6.97 ± 0.81	0-5 P(3)	1402.6484	25.39 ± 1.11	2-2 P(11)	1248.1447	1.24 ± 0.33
1-8 R(6)	1556.8600	4.97 ± 0.71	0-6 P(3)	1463.8260	18.59 ± 1.06	2-5 P(11)	1412.8123	1.32 ± 0.37
Fluoresced by 1-2 P(5) λ 1216.0696			0-7 P(3)	1525.1532	7.50 ± 0.76	2-8 P(11)	1572.6868	4.73 ± 0.79
1-3 P(5)	1271.9246	2.99 ± 0.46	0-3 R(1)	1274.9215	5.96 ± 0.58	2-9 P(11)	1620.0932	3.77 ± 1.05
1-5 P(5)	1387.3618	1.57 ± 0.36	0-4 R(1)	1333.7974	6.08 ± 0.55	2-5 R(9)	1381.9545	1.63 ± 0.35
1-6 P(5)	1446.1175	9.10 ± 0.86	0-5 R(1)	1393.9613	14.70 ± 0.92	2-6 R(9)	1436.8059	1.95 ± 0.39
1-7 P(5)	1504.7509	15.64 ± 1.17	0-6 R(1)	1454.9710	10.21 ± 0.92	2-9 R(9)	1592.1893	4.84 ± 0.84
1-8 P(5)	1562.3886	8.74 ± 0.98	0-7 R(1)	1516.2181	5.27 ± 1.58	Fluoresced by 2-2 P(8) λ 1219.1543		
1-3 R(3)	1257.8277	2.47 ± 0.47	Fluoresced by 2-1 P(13) λ 1217.9041			2-5 P(8)	1384.7720	1.80 ± 0.34
1-4 R(3)	1314.6130	1.76 ± 0.37	2-2 P(13)	1271.1773	4.18 ± 0.60	2-6 P(8)	1440.8746	1.48 ± 0.42
1-6 R(3)	1431.0102	6.34 ± 0.76	2-3 P(13)	1325.3415	1.21 ± 0.30	2-8 P(8)	1550.2888	3.78 ± 0.90
1-7 R(3)	1489.5637	10.70 ± 0.97	2-4 P(13)	1379.9818	1.91 ± 0.41	2-9 P(8)	1601.3989	5.52 ± 1.27
1-8 R(3)	1547.3337	6.93 ± 0.92	2-5 P(13)	1434.5327	6.44 ± 0.63	2-5 R(6)	1361.6294	2.51 ± 0.42
1-9 R(3)	1603.2490	4.73 ± 1.01	2-6 P(13)	1488.2389	4.11 ± 0.68	2-6 R(6)	1417.5063	1.90 ± 0.42
Fluoresced by 3-3 P(1) λ 1217.0377			2-7 P(13)	1540.0937	3.21 ± 0.59	2-8 R(6)	1527.3823	1.90 ± 0.48
3-7 P(1)	1435.0477	1.05 ± 0.32	2-8 P(13)	1588.7925	15.49 ± 1.39	2-9 R(6)	1579.4050	5.40 ± 0.87
3-10 P(1)	1591.3101	4.72 ± 0.83	2-9 P(13)	1632.6080	8.90 ± 1.36	2-10 R(6)	1627.6722	2.48 ± 0.67
Fluoresced by 0-2 R(0) λ 1217.2045			2-2 R(11)	1237.5357	3.13 ± 0.50	Fluoresced by 0-2 P(1) λ 1219.3676		
0-3 P(2)	1279.4639	4.08 ± 0.45	2-3 R(11)	1290.8972	3.47 ± 0.41	0-3 P(1)	1276.8127	4.01 ± 0.49
0-4 P(2)	1338.5682	16.33 ± 0.81	2-5 R(11)	1399.2344	6.50 ± 0.64	0-4 P(1)	1335.8675	8.94 ± 0.71
0-5 P(2)	1398.9514	17.08 ± 1.02	2-6 R(11)	1453.0927	6.34 ± 0.63	0-5 P(1)	1396.2225	5.67 ± 0.55
0-6 P(2)	1460.1650	11.48 ± 0.97	2-8 R(11)	1555.8804	9.85 ± 0.98	0-6 P(1)	1457.4346	6.97 ± 0.63
0-7 P(2)	1521.5869	4.07 ± 0.72	2-9 R(11)	1602.2641	16.48 ± 1.70	0-7 P(1)	1518.8937	3.63 ± 0.78
0-3 R(0)	1274.5343	4.42 ± 0.51	2-10 R(11)	1642.9363	4.76 ± 1.04	Fluoresced by 0-1 R(11) λ 1219.7454		
0-4 R(0)	1333.4741	6.44 ± 0.57	Fluoresced by 2-1 R(14) λ 1218.5205			0-5 P(13)	1485.4157	1.86 ± 0.46
0-5 R(0)	1393.7190	8.11 ± 0.73	2-1 P(16)	1257.3939	1.27 ± 0.29	0-3 R(11)	1331.9550	0.65 ± 0.26
0-6 R(0)	1454.8287	3.46 ± 0.59	2-2 P(16)	1310.5466	2.14 ± 0.39	0-4 R(11)	1389.5844	1.79 ± 0.46
0-7 R(0)	1516.1972	2.28 ± 0.68	2-5 P(16)	1470.4409	2.40 ± 0.54			
			2-8 P(16)	1612.3812	4.63 ± 1.03			
			2-2 R(14)	1270.7436	1.77 ± 0.75			
			2-3 R(14)	1323.6694	1.09 ± 0.31			
			2-5 R(14)	1429.7062	1.85 ± 0.42			
			2-6 R(14)	1481.4176	1.27 ± 0.32			
			2-8 R(14)	1576.8729	4.39 ± 0.74			